Wave patterns in frequency-entrained oscillator lattices

Jan Eric Sträng*
Abteilung Theoretische Physik, Universität Ulm, Albert-Einstein-Allee 11, D-89069 Ulm, Germany

Per Östborn†
Division of Mathematical Physics, Lund University, S-221 00 Lund, Sweden
(Received 22 March 2005; published 30 November 2005)

We study and classify firing waves in two-dimensional oscillator lattices. To do so, we simulate a pulse-coupled oscillator model aimed to resemble a group of pacemaker cells in the heart. The oscillators are assigned random natural frequencies, and we focus on frequency entrained states. Depending on the initial condition, three types of wave landscapes are seen asymptotically. A *concentric landscape* contains concentric waves with one or more foci. *Spiral landscapes* contain one or more spiral waves. A *mixed landscape* contains both concentric and spiral waves. Mixed landscapes are only seen for moderate coupling strengths g, since for higher g, spiral waves have higher frequency than concentric waves, so that they cannot mix in frequency entrained states. If the initial condition is random, the probability to get a concentric landscape increases with increasing coupling strength g, but decreases with increasing lattice size. The g dependence of the probability enables hysteresis, where the system jumps between the two landscape types as g is continuously changed. For moderate g, spiral tips rotate around a suppressed oscillator that never fires. We call such an oscillator an *oscillator defect*. A spiral may also rotate around a *point defect* situated between the oscillators. In that case all oscillators fire at the entrained frequency. For larger g, a spiral tip either moves around a row of suppressed oscillators, a *row defect*, or around an open curve situated between the oscillators, which may be called a *line defect*. The length of a row or line defect increases with g. Our results may help understand sinus node reentry, where the natural pacemaker of the heart suddenly shifts to a higher frequency. Some of the observed phenomena seem generic, based on simulations of other models.

DOI: 10.1103/PhysRevE.72.056137 PACS number(s): 05.65.+b, 87.18.Hf, 05.45.−a

I. INTRODUCTION

Networks containing a large number N of limit cycle oscillators appear in many areas of science [1]. Examples are pacemaker cells in the brain and heart, swarms of fireflies, and applauding audiences. There have been large efforts to understand the collective dynamics of such systems. Mathematical analysis is easiest if the oscillators are identical or are coupled all-to-all [2,3]. In the applications, however, oscillator networks tend to have spatial structure and consist of units with diverse natural frequencies. There are few analytical results applying to such systems [4–6], and to a large extent, we still have to rely on numerical simulations to explore their dynamics.

We have previously simulated a two-dimensional square lattice of diverse oscillators aimed to resemble pacemaker cells in the heart [7]. As coupling strength increases, we found two phase transitions in the thermodynamic limit $N\to\infty$. At the first transition, the largest frequency entrained oscillator cluster becomes infinite. At the second, global frequency entrainment settles.

In this paper, we study the same system in the frequency entrained regime. In the biological applications, many oscillator communities operate here. This is the case for the sinus node, which is the natural pacemaker of the heart [8]. It probably consists of millions of pacemaker cells. Frequency entrainment is also present in epileptic brain tissue [9], in cell groups responsible for the circadian rhythm [10] and locomotion [11], in the electric organ of weakly electric fish [12], and in some species of fireflies [13].

The purpose of the present paper is to study *firing waves* in this kind of system. Biological oscillators can often be described as *integrate and fire* oscillators, which fire pulses at a natural frequency. In the case of pacemaker cells in the heart, the pulses are electrical, and perturb the rhythmic activity of neighbor cells. The pulses may also be light flashes, chemical signals, acoustic waves, or have some other nature. The firing of one oscillator often triggers the firing of its neighbors, so that a firing wave is formed.

Generally, waves in oscillatory media can be described as waves in the phase field. The phase at some point in the medium is the position in the oscillation cycle of this point. Most studies of such waves deal with continuous media [1,14], such as the Belousov-Zhabotinsky reaction in a thin fluid film [15] and the Ginzburg-Landau model [16]. Both concentric and spiral waves have been observed. A spiral wave implies a phase singularity, a point in the medium where the phase cannot be defined. Recently, interest has focused on spiral waves with line defects, where the phase is discontinuous along a curve [17]. In these continuous media, the natural frequency of oscillation is most often assumed to be homogeneous. In discrete media, where the oscillators have diverse natural frequencies, some examples of concentric waves [18] and spirals [19] have been reported in frequency entrained lattices. However, to our knowledge, no

*Electronic address: eric.straeng@uni-ulm.de
†Electronic address: per.ostborn@matfys.lth.se

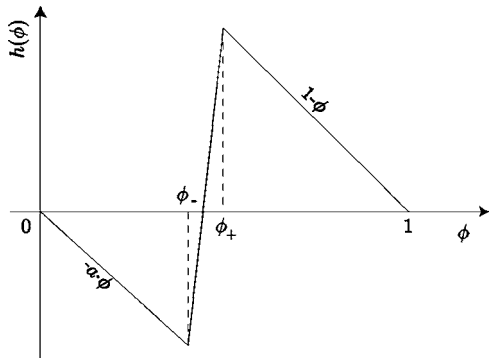

FIG. 1. The phase response curve (PRC) $h(\phi)$ used in model (1). It gives rise to diffusive coupling, which tends to decrease phase differences between neighbor oscillators. We use $a=1$, $\phi_-=0.4$, and $\phi_+=0.5$.

systematic study of wave patterns in this kind of system has been performed. The present study is an attempt in this direction.

The model we use is particularly suited to study the sinus node. Experimentally, a single concentric wave in the sinus node is found to initiate the normal heartbeat [8]. However, in the cardiac condition known as *sinus node reentry*, an excitation wave that circles around the sinus node is found [20]. This suggests the presence of one or more spirals inside the node. Also, the beating frequency of the heart suddenly increases. We will see that some of our results may have relevance to this condition.

II. MODEL AND NUMERICAL METHODS

We consider oscillators placed on a square, two-dimensional lattice. The state of each oscillator is given by the phase $0 \leqslant \phi_{ij} < 1$. The equation of motion of the system can be written

$$\dot{\phi}_{ij} = \frac{1}{\pi_{ij}} + gh(\phi_{ij}) \sum_{kl \in n_{ij}} \delta(\phi_{kl}). \tag{1}$$

The natural periods π_{ij} are random numbers from a uniform distribution with $\pi_{\min}=1.0$ time units (tu) and $\pi_{\max}=1.5$ tu. The oscillators interact bidirectionally with their nearest neighbors, so that $n_{ij}=\{(i+1,j),(i-1,j),(i,j+1),(i,j-1)\}$. An oscillator (k,l) is said to *fire* when $\phi_{kl}=1$. Then $\phi_{kl} \mapsto 0$ and pulses are delivered to its neighbors, perturbing them according to $\phi_{ij} \mapsto \phi_{ij}+gh(\phi_{ij})$. Here, g is the coupling strength and $h(\phi)$ is the phase response curve (PRC).

Our choice of PRC (Fig. 1) approximates the response of a cardiac pacemaker cell to a brief electric current, coming, e.g., from a neighbor cell that fires an action potential [21]. From the requirement $0 \leqslant \phi + gh(\phi) < 1$, it follows that $0 \leqslant g < 1$. If $g=1$ and $\phi_{ij} > \phi_+$, a pulse delivered to oscillator (i,j) will immediately bring this oscillator to the firing state. This corresponds to an infinitely fast transmission of firing waves and, therefore, to infinitely strong coupling.

The method of integration is the same as in Ref. [7]. In the one-dimensional case, the method is described in detail in Ref. [5]. The lattice is divided into blocks of 10×10 oscillators. After each time increment $\Delta t=0.01$, we let $\phi_{ij} \mapsto \phi_{ij}+\Delta t/\pi_{ij}$ for all oscillators (i,j). Then the blocks are checked in a predefined order. There may be some oscillators in a block that is currently checked that have $\phi_{ij}>1$. These have fired at some point in time after the previous time increment. The phase of the oscillator in the block that must have fired *first* is reduced by 1, and pulses are delivered to its neighbors. Then the oscillator that must have fired *second to first* is handled, and so on, until $\phi_{ij}<1$ for all oscillators within the block. Then the algorithm moves on to the next block. This algorithm becomes an exact method of integration if the block size is the same as the lattice size. The other extreme is that a block consists of a single oscillator. Then all oscillators are checked for firings and handled in a predefined scanning order. This may introduce errors if several oscillators fire within the same time step. This situation occurs quite often in this study, since we consider high g, leading to a high degree of coherence.

We found that the block method was essential to get accurate results in reasonable time for $g>0.8$. To check the accuracy, we used exact integration to simulate lattices of sizes 50×50 and 100×100 for reference, and then used the same assignment of natural periods and the same initial condition in different inexact integration schemes. With the block method, the emerging phase landscapes (see below) were always the same as the true ones, in the sense that the positions and numbers of foci and spirals did not change. However, small deviations of the individual phases at a given time could be found. In principle, the block method may introduce a length scale related to the side length of the block. However, no signs of such length scales were found, based on visual inspection of phase landscapes produced with different block sizes. In contrast, for too small block sizes, artifacts from the scanning order of the lattice were clearly visible for high g, and spirals and foci were displaced. Of course, errors are reduced if Δt is reduced, but too long computation times were then needed to get accurate results. Exact integration is also unfeasible to use throughout the study, since the integration time is then $\propto N^2$, where N is the number of oscillators. The reason is that during each period of oscillation, the firing of N oscillators must be handled, and for each firing, all N oscillators must be checked to find the one that is to fire first. Nevertheless, using a reduced number of data points, we checked that Figs. 3 and 7 got the same appearance with exact integration.

In the frequency entrained regime, the overall structure of the wave pattern stabilizes within a transient of 1000 tu for the lattice sizes we use. However, the stabilization time depends on g. Unless otherwise stated, measurements were made after a transient of 5000 tu.

To produce statistics of the model behavior, we use random initial conditions, where each $\phi_{ij}(t=0)$ is an independent random number, uniformly distributed in the interval [0,1). Both open and periodic boundary conditions are used.

III. RESULTS

A. General

We will call the discrete field $\phi(i,j,t)=\phi_{ij}(t)$ a *phase landscape*, or just a *landscape*. As expected in oscillatory

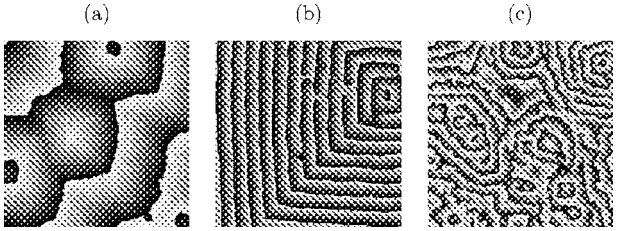

FIG. 2. The three different types of phase landscapes. (a) Concentric landscape for $g=0.9$. (b) Spiral landscape for $g=0.9$. (c) Mixed landscape for $g=0.57$. Black corresponds to $\phi=0$ and white to $\phi=1$.

media, the phase landscapes exhibit wave patterns. We may define a *wave front* to be a curve that runs between the oscillators in the lattice, such that the phases of all oscillators adjacent to the curve on one side are close to 1, and the phases of all oscillators on the other side are close to 0. Naturally, a wave front moves in the direction where the phases gradually decrease from 1. Two wave fronts that meet annihilate each other (Sec. IV B).

In frequency entrained lattices, we find three basic types of stable phase landscapes (Fig. 2). A *concentric landscape* consists of one or more concentric waves that move outward from a focus. A concentric focus may be defined as an oscillator (i,j) that triggers the firings of all eight oscillators (k,l) that surround (i,j). In other words, $\phi_+ < \phi_{kl} < 1$ just before (i,j) fires for all eight oscillators (k,l).

The *spiral landscapes* consist of one or more spiral waves that spiral outward from the tip. Each interior end point of a wave front corresponds to a spiral. In a continuous two-dimensional medium, a point p is a spiral tip if

$$\oint_c \nabla \phi \cdot dl = m, \quad m = \pm 1, \pm 2, \pm 3, \ldots, \tag{2}$$

where the closed curve c encircles p and is small enough. If we require that c is run through clockwise, a positive m corresponds to a spiral that rotates anticlockwise, and a negative m to a spiral rotating clockwise. In a discrete medium, the integral should be replaced by a summation of phase differences between neighbor oscillators (i,j) and (k,l) along a closed path c. The minimum phase difference should be used, i.e., $\min\{\phi_{kl}-\phi_{ij}, 1-(\phi_{kl}-\phi_{ij})\}$. We have only come across spirals with multiplicity of 1, i.e., $m=\pm 1$.

Finally, a *mixed landscape* contains both concentric and spiral waves.

In the region $g_{c2} < g < 1$, we only find frequency entrained states. (A possible exception is discussed in Sec. III E.) Here, $g_{c2} \approx 0.56$ is the critical coupling at which frequency entrainment first appears in the thermodynamic limit $N \to \infty$ [7]. In other words, there seems to be no bistability between frequency entrained states and other types of states. This means that the phase landscape always seems to repeat itself exactly at the entrained frequency.

In a statistical sense, the behavior of the model seems to be the same in the two cases of open and periodic boundary conditions. However, the topological constraints on the phase landscapes are somewhat different (Sec. IV A).

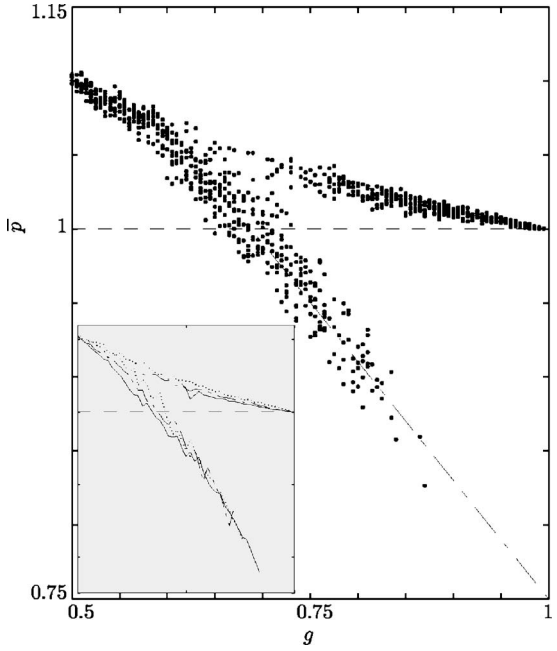

FIG. 3. Mean firing periods $\bar{p}$. Ten realizations were simulated for each g. The lattice size was 100×100. Points on the upper arm come from concentric landscapes and points on the lower arm come from spiral landscapes. Inset: Average $\bar{p}$, calculated from ten realizations, for the lattice sizes 50×50 (dotted line), 100×100 (dash-dotted line), and 200×200 (solid line). Averages are taken for concentric landscapes separately from the other two landscape types.

Figure 3 shows the lattice and time mean $\bar{p}$ of the firing periods p_{ij}, in an interval of coupling strengths g that contains the region where frequency entrainment is present. Each point corresponds to a statistically independent realization with random natural periods and a random initial condition. Above $g \approx 0.7$, the points fall on one of two clearly distinguishable arms. All points on the upper arm correspond to concentric landscapes, and those on the lower arm correspond to spiral landscapes. This conclusion is based on visual inspection of the phase landscapes, and on algorithms counting the number of concentric foci and spirals in each landscape (cf. Figs. 10, 14, and 15). For lower values of g, where the arms merge, we find all three types of phase landscapes (concentric, spirals, and mixed). It is important to note that for a given assignment of natural periods and a given g, all the allowed types of phase landscapes can be obtained by just varying the initial condition. The upper arm seems to converge at $\bar{p}=1$ as $g \to 1$. If we extrapolate the lower arm toward $g=1$, it seems to converge at $\bar{p}=0.75$. These findings are discussed in Sec. IV C.

The inset in Fig. 3 shows averages of $\bar{p}$ as functions of g for three different lattice sizes. We see that the results are essentially size independent. Though, it seems that in concentric landscapes, the entrained period comes closer to one when the lattice size grows. It also seems that the lower arm becomes more straight.

It may be noted in Fig. 3 that more and more points seem to fall on the upper arm as g increases. Figure 4(a) more clearly shows that the probability to find a concentric landscape increases with g. It is also seen that the probability to

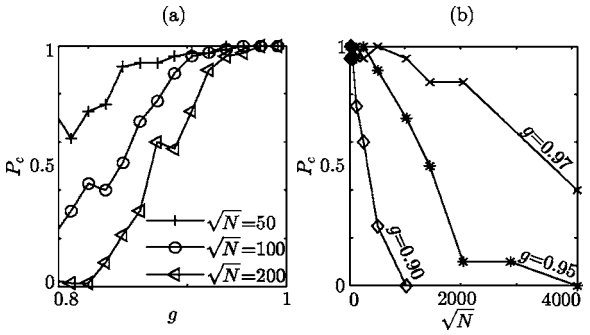

FIG. 4. (a) The probability P_c to find a concentric landscape as a function of g for three different lattice sizes N. (b) P_c as a function of the lattice side length $\sqrt{N}$ for three different values of g. Each probability is estimated from a sample of 20 realizations.

find a concentric landscape decreases with increasing lattice size. This is more clearly seen in Fig. 4(b). These two panels give some support to three additional hypotheses: (1) For each $g<1$ in the frequency entrained regime and each lattice size N, there is a nonzero probability P_c to have a concentric landscape and a nonzero probability P_s to have a spiral landscape. (2) For any given N, $P_c \to 1$ as $g \to 1$. (3) For any given $g<1$, $P_c \to 0$ as $N \to \infty$. (As discussed above, mixed landscapes seem to be forbidden for high enough coupling, so that $P_c+P_s=1$.)

B. Coherence

In the globally coupled Kuramoto model, the onset of partial frequency entrainment and partial coherence occurs at the same critical coupling in the thermodynamic limit $N \to \infty$. The degree of coherence is often measured by means of the complex order parameter

$$z(t) = \frac{1}{N}\sum_{k=1}^{N} e^{2\pi i \phi_k(t)}. \tag{3}$$

Partial coherence means that $|z| \neq 0$, and $|z|=1$ corresponds to perfect coherence.

In locally coupled networks, the existence of waves in the phase landscape suggests that we can have frequency entrainment without coherence. Nevertheless, it might be interesting to study a coherence measure similar to (3) in our system. Partial coherence is expected when the wavelength is larger than the side length of the lattice. We choose to study the following quantity:

$$s(t) = \frac{1}{N}\sum_{ij} e^{2\pi i \phi_{ij}(t) \pi_{ij}}. \tag{4}$$

The factor π_{ij} causes all exponents in the sum to grow with the same speed between the firings, producing a measure that is more well behaved than (3) in our model. The evolution of $s(t)$ in the complex plane resembles that of a limit cycle. It approaches a closed curve, to which it returns if the system is perturbed. In Fig. 5, we see that concentric and spiral landscapes have different coherence signatures. The circle traced out by $s(t)$ in a concentric landscape is approximately centered at the origin, whereas this is not the case in a spiral landscape. Further, at a given coupling strength g, the concentric circle has a larger area than the corresponding spiral circle, which is also more deformed. If we let g approach 1, the coherence becomes almost perfect in concentric landscapes.

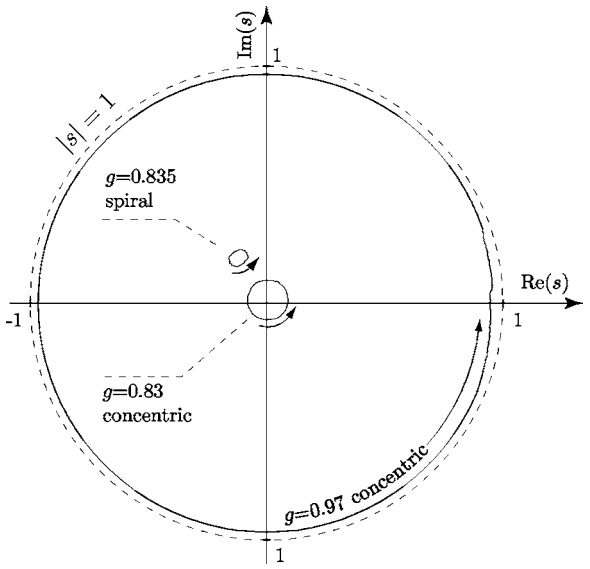

FIG. 5. The evolution of the complex order parameter s [Eq. (4)] during one period of oscillation for three different phase landscapes.

Since some circles are not centered at the origin, the radius $|s|$ is not a suitable measure of the degree of coherence. Instead, we use A/π, where A is the area circled by $s(t)$. Perfect coherence corresponds to $A/\pi=1$. Figure 6(a) shows this measure for a set of independent realizations, in the same way as in Fig. 3. Again, two arms separate at $g \approx 0.7$. The areas in the upper arm grows smoothly toward 1 and come from concentric landscapes. The areas in the lower arm stay small in the range of g values in which we can observe it and come from spiral landscapes. Figure 6(b) shows mean areas for three different lattice sizes. We see that the transition region in which the area grows rapidly moves toward

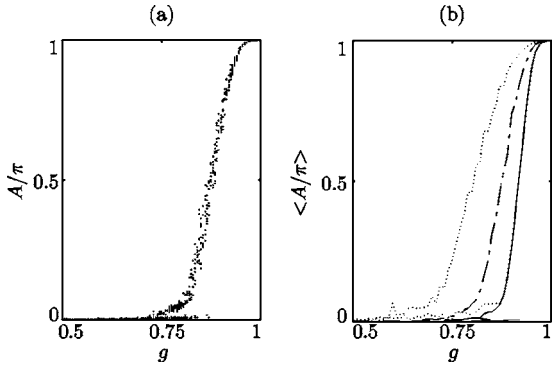

FIG. 6. Normalized area A/π circled by the order parameter s. (a) Ten realizations simulated for each g in a 100×100 lattice. (b) Area averages in a sample of ten realizations for the lattice sizes 50×50 (dotted line), 100×100 (dash-dotted line), and 200×200 (solid line). Averages are taken for concentric landscapes and other landscape types separately.

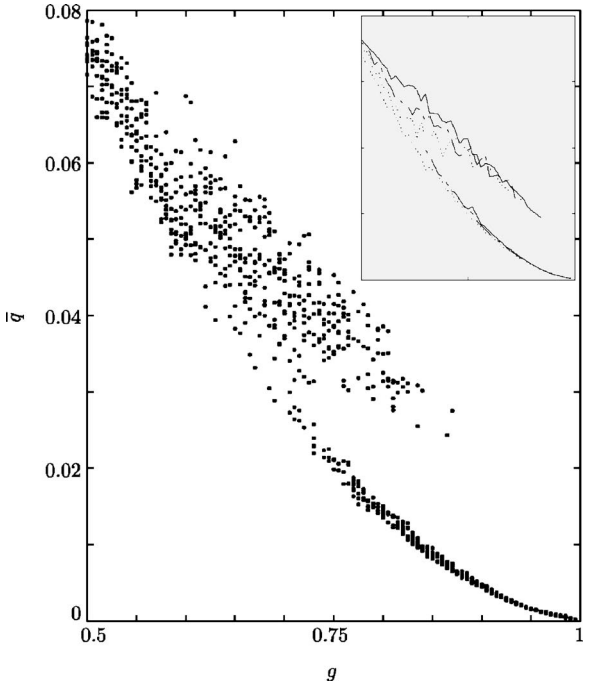

FIG. 7. The local coherence measure $\bar{q}$ [Eq. (5)]. Ten realizations were simulated for each g in a 100×100 lattice. Points on the upper arm come from spiral landscapes and points on the lower arm come from concentric landscapes. Inset: Averages in a sample of ten realizations for the lattice sizes 50×50 (dotted line), 100×100 (dash-dotted line), and 200×200 (solid line).

higher g when the lattice size increases. This suggests that $A/\pi\to0$ for all $g<1$ in the thermodynamic limit $N\to\infty$. Therefore, there does not seem to be any phase transition toward coherence at a finite coupling strength ($g<1$).

This finding is easily explained if we assume that the wavelength is independent of N and there is a single concentric focus at large values of g, regardless the lattice size (Sec. V). Then, a given g corresponds to a specific wavelength, and a sufficiently large lattice will contain many wave fronts. Consequently, there will be little coherence. To be able to study the wavelength, we introduce a measure $\bar{q}$ of the mean time lag between firings of neighbor oscillators. The inverse of such a measure should be roughly proportional to the wavelength. We store the last firing instant T_{ij} for each oscillator (i,j) before some time limit $T_{\max}$. Then

$$q_{ij}=\left\langle \min\left\{\frac{|T_{ij}-T_{kl}|}{\bar{p}},\quad 1-\frac{|T_{ij}-T_{kl}|}{\bar{p}}\right\}\right\rangle_{kl\in n_{ij}}, \qquad (5)$$

where n_{ij} is the set of nearest neighbors to oscillator (i,j), as defined in Sec. II. We then let $\bar{q}=\langle q_{ij}\rangle$ be the lattice mean of q_{ij}. Contributions from quiescent oscillators are excluded. Figure 7 shows $\bar{q}$ for a set of independent realizations. Just as for $\bar{p}$ in Fig. 3, the points fall on either of two clearly separated arms above $g\approx0.7$. In this case, the points on the lower arm correspond to concentric landscapes, and those on the upper arm correspond to spiral landscapes. This was concluded in the same way as for the data in Fig. 3. The inset in Fig. 7 shows averages for different lattice sizes in the same way as in Figs. 3 and 6. The results are essentially lattice size independent. In particular, this is true for the concentric landscapes at high g. We find that the three curves are well fitted to the same parabola $\bar{q}=(1/4)(1-g)^2$. The exponent 2 may be interpreted as a critical exponent. Just as in Fig. 3, the arm corresponding to spiral landscapes becomes more straight in larger lattices and does not seem to converge at $\bar{q}=0$ as $g\to1$. However, for theoretical reasons, this must be the case, provided spiral landscapes exist in this limit (Sec. IV C).

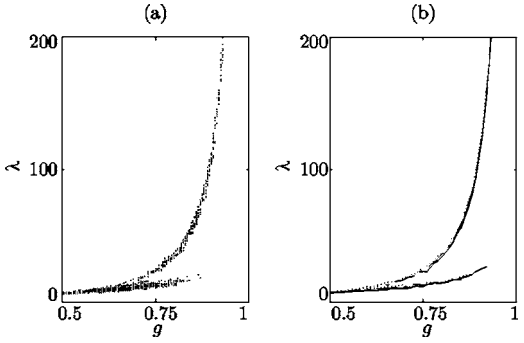

FIG. 8. Estimation of the wavelength as $\lambda\approx1/(2\bar{q})$. (a) Ten realizations simulated for each g in a 100×100 lattice. (b) Averages in a sample of ten realizations for the lattice sizes 50×50 (dotted line), 100×100 (dash-dotted line), and 200×200 (solid line).

To estimate the wavelength, we use $\lambda\approx1/(2\bar{q})$. This approximation is exact if we are dealing with plane waves that move horizontally or vertically. In true phase landscapes, some factor between 1 and 2 should be inserted in the denominator, depending on the curvature of the waves. Our approximation is acceptable, however, comparing with wavelengths measured by hand or with the help of the two-dimensional Fourier transform. Figure 8 shows these wavelength approximations. The fact that they are independent of the lattice size (cf. Fig. 7) conforms with the finding that the degree of coherence decreases when the lattice size grows (Fig. 6). From the discussion of Fig. 7, we immediately deduce that the wavelength of concentric landscapes diverges according to $\lambda\propto(1-g)^{-2}$ as $g\to1$. As discussed above, and in Sec. IV C, the wavelength of spiral landscapes must also diverge, if they exist in this limit.

C. Concentric landscapes

Simulations with the same assignment of natural periods, but different initial conditions, strongly suggest that there is only one stable concentric phase landscape at a given g. In other words, the system seems to have only one attractor corresponding to a concentric landscape in the frequency entrained regime. (Of course, some initial conditions drive the system toward other attractors, containing spirals.) This is not very surprising, since there is only one frequency entrained state in the corresponding one-dimensional oscillator chain [7] of the kind that corresponds to the concentric landscapes seen in the simulations.

We also find strong correlations between the concentric landscapes arising from the same assignment of natural periods, but from different g (Fig. 9).

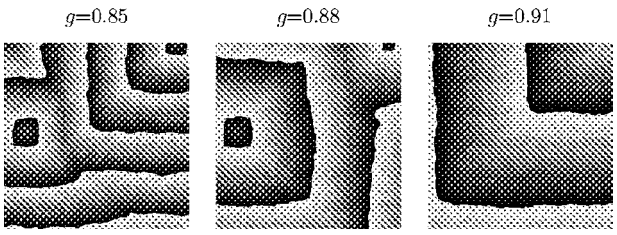

FIG. 9. Concentric phase landscapes arising from different coupling strengths g, but from the same assignment of natural periods. The landscapes are strongly correlated. Lattice size 300×300.

Figure 10(a) shows the number of foci in a set of independent realizations. A focus is defined as in Sec. III A. At a first glance, the numbers seem unreasonably large, compared to the visual impression of concentric phase landscapes (Fig. 9). The reason is that most foci have a very little "area of influence," meaning that the closed wave front emanating from the focus does not have time to grow large before it is swallowed by a larger closed wave front, emanating from another focus. Therefore, these small concentric waves are most often not seen in snapshots of the phase landscape. Nevertheless, the large focus numbers seemingly drop toward 1 as $g\rightarrow1$.

Figure 10(b) shows average focus densities for three different lattice sizes. Curiously, the focus density drops when the lattice size increases. This is interesting in the context of the seemingly absent phase transition toward coherence. If the focus density was independent of N, or increased, the degree of coherence could remain nonzero as $N\rightarrow\infty$ (Sec. V).

D. Spiral and mixed landscapes

When the initial condition is varied randomly for a given assignment of natural periods and a given g, all concentric phase landscapes that arise seem identical (Sec. III C). In contrast, most phase landscapes with spirals that arise do not seem correlated at all (Fig. 11).

However, some of these phase landscapes containing spirals are strongly correlated with the corresponding concentric

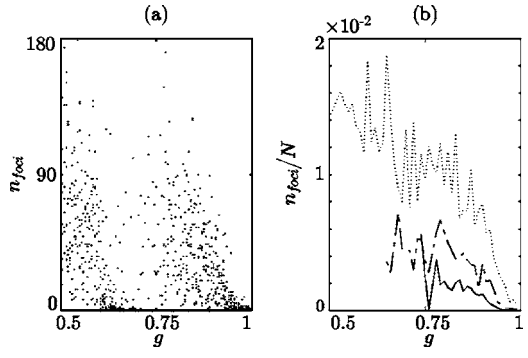

FIG. 10. The number n_{foci} of concentric foci. (a) Ten realizations simulated for each g in a 100×100 lattice. (b) Average focus densities in a sample of ten realizations for the lattice sizes 50×50 (dotted line), 100×100 (dash-dotted line), and 200×200 (solid line). The averages are taken for concentric landscapes.

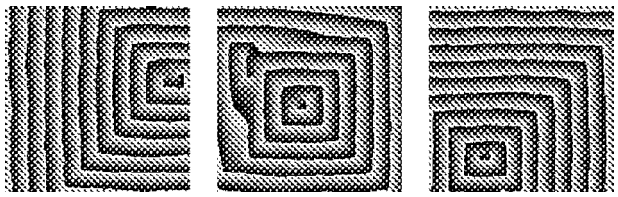

FIG. 11. Spiral phase landscapes arising from the same coupling strength $g=0.9$, the same assignment of natural periods, but from different initial conditions. The landscapes do not seem correlated. Lattice size 200×200.

landscapes (Fig. 12). The probability to get such correlated landscapes seems to decrease as g increases. It seems that both mixed and purely spiral landscapes can be both correlated and uncorrelated. However, we are not certain that purely spiral landscapes at high g with $\bar{p}<1$ can be correlated with the corresponding concentric landscape, since candidates for such correlated landscapes arise very rarely at these high values of g. Therefore, the apparent correlations might be accidental. A more thorough statistical investigation, using a quantity measuring the degree of correlation between the two landscapes, would be necessary to resolve these questions.

The probability to get correlated landscapes containing spirals seems to decrease quickly when the lattice size increases. They appear often in 50×50 lattices, but very seldom in 100×100 lattices. Nevertheless, if the initial condition is carefully chosen, they can be seen in very large lattices also. Figure 12 shows an example in a 300×300 lattice, where the initial condition $\phi_{ij}=0$, $\forall ij$ is used for two different values of g.

We have come across several kinds of spirals. They may have different global characteristics or different local dynamics close to the spiral tip. Let us first distinguish between two kinds of global wave front topologies. A spiral may either act as a focus, like the double spiral in the upper right corner of Fig. 2(b), or it may be "enslaved." Such a spiral is often sandwiched between two wave fronts, like all other interior end points of the wave fronts in Fig. 2(b). These two kinds of spirals are defined in Fig. 13.

Let us turn to the spiral tip dynamics. In a continuous oscillatory medium, a stationary spiral tip corresponds to a point where the phase cannot be defined. As we approach

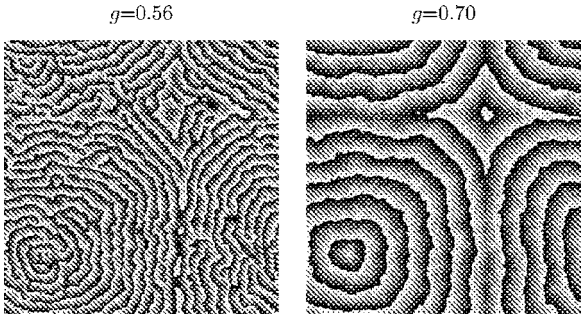

FIG. 12. Mixed and concentric phase landscapes arising from the same assignment of natural periods, but from different g. The landscapes are strongly correlated. Lattice size 300×300.

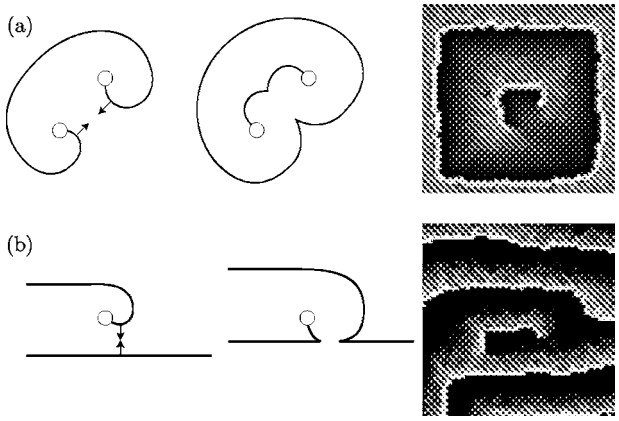

FIG. 13. Two kinds of global spiral topologies. (a) The wave front emanating from the spiral tip (ring) collides with itself. (b) The wave front emanating from the spiral tip collides with another wave front.

this phase singularity, the amplitude of the oscillation goes to zero. In a discrete lattice, a stationary spiral tip may either be placed *between* the oscillators or *on* one of the oscillators. In the first case, the wave front circles a block of 2×2 oscillators, as shown in Fig. 21(a1). We will say that the wave front circles a *point defect*. In the second case, the wave front circles a suppressed oscillator (i,j) that never fires [Fig. 21(b1)]. The suppressed oscillator has a phase $0<\phi_{ij}<\phi_-$, and when the four neighbors fire in consecutive order, ϕ_{ij} jumps backward each time, since $h(\phi_{ij})<0$, so that the phase is kept in this interval (Sec. IV D).

Figure 14(a) shows the number of point defects in a set of independent realizations of the system. The number decreases as g increases and becomes zero in most realizations above $g\approx0.6$. Figure 14(b) shows average defect densities for different lattice sizes. There is a weak tendency that the defect density increases with the lattice size. The point defects are identified in the following way: Each block of 2×2 oscillators is investigated. If we go around such a block in a closed path and pass exactly one wave front, then there is a point defect in the middle of that block. To judge how

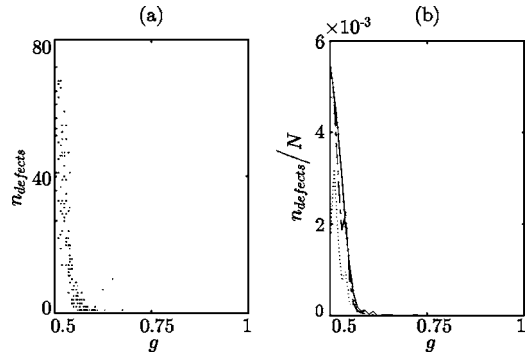

FIG. 14. The number $n_{defects}$ of point defects. (a) Ten realizations simulated for each g in a 100×100 lattice. (b) Average defect densities in a sample of ten realizations for the lattice sizes 50×50 (dotted line), 100×100 (dash-dotted line), and 200×200 (solid line). The averages are taken for those phase landscapes that contain spirals.

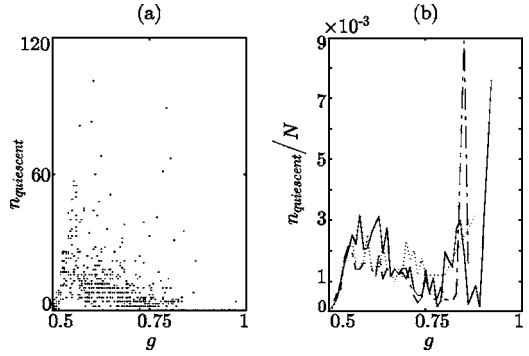

FIG. 15. The number $n_{quiescent}$ of quiescent oscillators. (a) Ten realizations simulated for each g in a 100×100 lattice. (b) Average quiescent oscillator densities in a sample of ten realizations for the lattice sizes 50×50 (dotted line), 100×100 (dash-dotted line), and 200×200 (solid line). The averages are taken for those phase landscapes that contain spirals.

many wave fronts we pass, the following time differences between the firings of the oscillators in the block are calculated [cf. Eq. (5)]:

$$\Delta T_1 = T_{i,j} - T_{i,j+1},$$

$$\Delta T_2 = T_{i,j+1} - T_{i+1,j+1},$$

$$\Delta T_3 = T_{i+1,j+1} - T_{i+1,j},$$

$$\Delta T_4 = T_{i+1,j} - T_{i,j}. \tag{6}$$

If $|\Delta T_k|>0.5\bar{p}$ for exactly one k, then we judge that the block contains a point defect. It was checked in several simulations that this method identifies the correct defects.

Figure 15(a) shows the number of quiescent oscillators in a set of independent realizations. They seem to be improbable for coupling strengths below $g\approx0.5$ and above $g\approx0.8$. The number of quiescent oscillators is essentially the same as the number of spirals encircling an oscillator defect (see below). Figure 15(b) shows average densities of quiescent oscillators. There is no clear indication that this density depends on the lattice size.

We also come across spirals with nonstationary tips. Sometimes the tip circles a fixed open curve [Fig. 21(a2)]. This curve may be called a *line defect* and is typically not straight, as shown in Fig. 16. In other cases, the spiral tip circles a given row of quiescent oscillators over and over again [Fig. 21(b2)]. This row may be called a *row defect*. We have come across spirals that rotate around curves consisting of pieces both of line defects and row defects.

Above $g\approx0.90$, the few spirals we encounter are exclusively of the nonstationary kind. It also seems that the length of the line or row defect increases with g. This is seen in Fig. 17. The reason for these facts is discussed in Sec. IV D. It seems that row defects are much more common than line defects.

Line defects are most often not detected by the algorithm used to find point defects [Eq. (6)], since they typically give $|\Delta T_k|>0.5\bar{p}$ for two different k. Since a row defect corre-

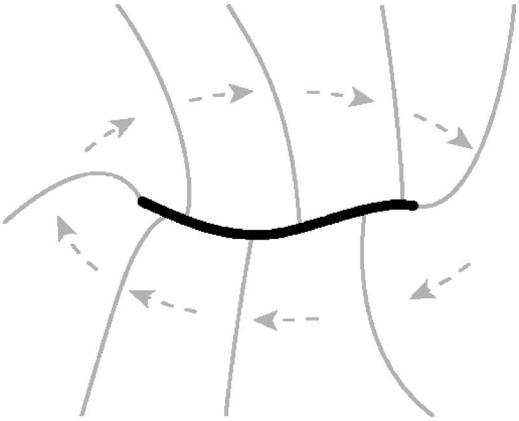

FIG. 16. A spiral wave front moving around a line or row defect.

sponds to a single spiral, the number of quiescent oscillators in Fig. 15 slightly overestimates the number of stationary spirals of this kind.

There are row defects that are not associated with spirals. An example is shown in Fig. 18. We have only come across such row defects in spiral landscapes. The reason may be that their frequency is higher, so that the quiescent oscillators can get pulses leading to backward phase jumps more often and more easily are kept quiescent.

E. Hysteresis

The fact that the probability to get concentric and spiral landscapes depends on coupling strength g (Fig. 4) opens the possibility of hysteresis effects. Assume that we have a spiral landscape acquired at some g. If we increase g gradually, it should be more and more improbable that the landscape stays on the spiral arm in Fig. 3. At some point it should jump to the concentric upper arm. If we then slowly decrease coupling, we should be able to stay on this arm. However, if coupling is reduced further, at some point we should jump down to the spiral arm again, since concentric landscapes then become more improbable. If we repeat this procedure, we should trace out a closed hysteresis curve over and over. This scenario is confirmed in simulations. The jump from the spiral to the concentric arm occurs at very high g. Depending on the time interval Δt between the changes in g, and the magnitude $|\Delta g|$ of these changes, the jump occurs somewhere between $g=0.96$ and $g=0.99$. This shows that there is a strong memory in the system, since it is very unlikely to get a spiral landscape from random initial conditions for such

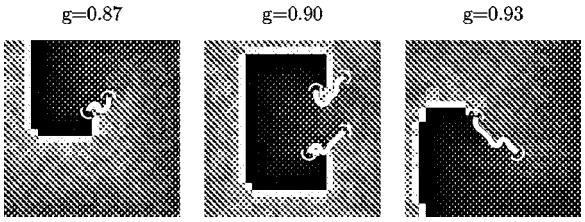

FIG. 17. Row defects at three different values of g. Their length seems to increase with g.

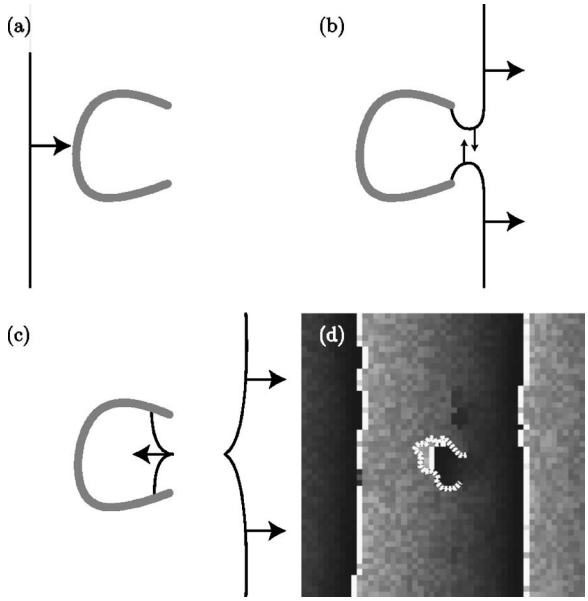

FIG. 18. A row defect that is not associated with a spiral. (a)–(c) Time evolution of a wave front passing the defect. (d) A piece of a phase landscape that contains this kind of defect.

g. Indeed, we see that the sequence of spiral phase landscapes that are produced in the process are strongly correlated. When high enough values of g are reached, we get spiral landscapes that seem unstable, in the following sense. If we fix g, the system does not reach a fully frequency entrained state even if we allow a transient as long as 10^5 tu. The phase landscape does not stabilize, and we see row defects that change place and shape continuously. This effect may be due to extremely long chaotic transients, reported in other kinds of extended media [22]. It may also be that there indeed exist nonfrequency entrained attractors in the frequency entrained regime.

F. Other models

We study model (1) in the form a one-dimensional oscillator chain with open ends, where each oscillator has the same characteristics as in the two-dimensional case. In a one-dimensional chain, no spirals are possible, of course [23]. In the frequency entrained regime, we only find frequency entrained phase landscapes with one or more foci corresponding to the states studied in Ref. [5]. The focus number decreases toward 1 as $g \to 1$. In contrast to the two-dimensional case, the focus density seems to be independent of the lattice size.

Figure 19(a) shows the mean period $\bar{p}$ in a set of independent realizations of the two-dimensional model with identical oscillators $\pi_{ij}=1$, $\forall ij$. All landscapes that appear are frequency entrained. The points in the horizontal upper arm correspond to coherent landscapes with $\bar{p}=1$. The lower arm corresponds to spiral landscapes. The curve apparently converges to $\bar{p}=0.5$ as $g \to 1$ (Sec. IV E). Just as in the case of diverse oscillators, the probability to get a spiral landscape seems to decrease when g increases, but seems to increase as the lattice size increases. Figure 19(b) shows the correspond-

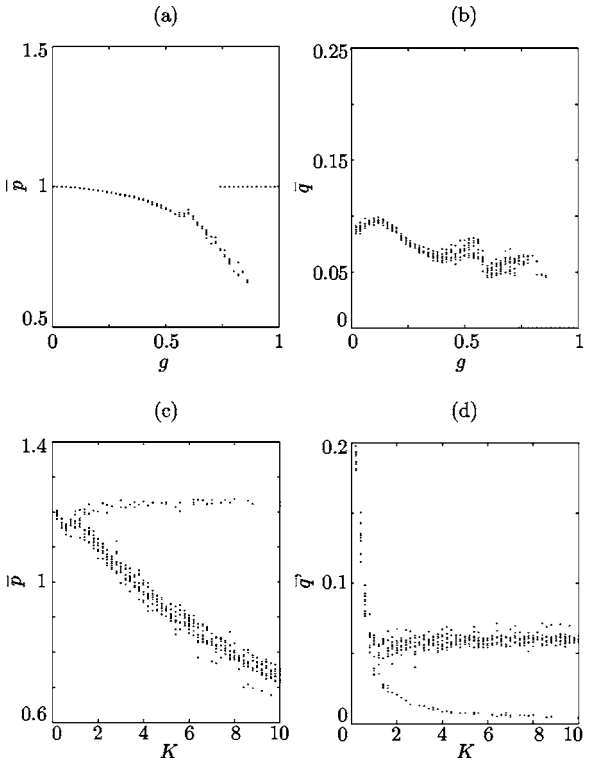

FIG. 19. Behavior of alternative models. (a) Mean firing periods $\bar{p}$ for the system (1) with identical oscillators $\pi_{ij}=1, \forall ij$. (b) Local coherence $\bar{q}$ for the same model. (c) Mean firing periods $\bar{p}$ for the system (7) with random natural periods $1.0 \leqslant \pi_{ij} \leqslant 1.5$. (d) Local coherence $\bar{q}'$ for the same model. In all panels, ten independent realizations are simulated for each coupling strength. In panels (a) and (b), the lattice size is 50×50, and in panels (c) and (d), it is 15×15.

ing values of $\bar{q}$. Coherent landscapes have $\bar{q}=0$, of course. The points in the upper, visible arm correspond to spiral landscapes. Below the dip at $g \approx 0.6$, all spirals seem to circle point defects, and above, they all seem to circle quiescent oscillators. No apparent correlations can be seen between spiral landscapes arising from the same g, the same assignment of natural periods, but different initial conditions.

To test the behavior of a radically different oscillator model, we study the system

$$\dot{\phi}_{ij} = \frac{1}{\pi_{ij}} + K \sum_{kl \in n_{ij}} \Gamma(\phi_{kl} - \phi_{ij}), \tag{7}$$

with $\Gamma(x)=\sin(2\pi x)+0.5\sin(2\pi x)^2$. This model is of the universal form that arises in the limits of small coupling and small oscillator diversity in any network of limit cycle oscillators [2]. The choice of coupling function $\Gamma(x)$ makes it plausible that a frequency entrained regime exists even as $N \to \infty$, since this is the case in the corresponding one-dimensional chain [6]. The natural periods are chosen in the same way as in the original model (1). Figure 19(c) shows $\bar{p}$ for a set of independent realizations. Two arms separate at $K \approx 0.8$. Frequency entrainment settles at a slightly lower K. Again, the points on the upper arm correspond to concentric landscapes, and those on the lower arm correspond to spiral landscapes. For lower values of the coupling strength, all three landscape types can be seen. No spirals circling quiescent oscillators are possible (Sec. IV E). Just as for system (1), the probability to get a concentric landscape seems to decrease as the lattice size increases. In model (7), it apparently decreases much quicker. In fact, it is hard to get concentric landscapes from random initial conditions with a lattice size larger than 15×15. (Though, they are consistently produced from homogeneous initial conditions.) In contrast to model (1), however, we see no clear trend that the probability to get a concentric landscape increases with the coupling strength. For this model, we define the local coherence measure as

$$q'_{ij} = \langle \min\{|\phi_{ij} - \phi_{kl}|, \quad 1 - |\phi_{ij} - \phi_{kl}|\} \rangle_{kl \in n_{ij}}, \tag{8}$$

letting $\bar{q}' = \langle q'_{ij} \rangle$. This measure is time independent in frequency entrained states. Figure 19(d) shows this quantity in a set of independent realizations. The points in the upper arm correspond to spiral landscapes and those in the lower to concentric landscapes. This arm approximately follows $\bar{q}' \propto K^{-1.1}$. Preliminary studies indicate that the correlation pattern between different landscape types is the same as for model (1) with diverse natural frequencies.

IV. THEORETICAL CONSIDERATIONS

A. Topological constraints

If ∂L is the lattice boundary, the integral $\oint_{\partial L} \nabla \phi \cdot dl$ must be zero if the boundary condition is periodic, whereas it can take any integer value if open boundary conditions are used. This means that the number of clockwise and anticlockwise spirals [cf. Eq. (2)] must be the same in any phase landscape with periodic boundary conditions and, in particular, that the number of spirals must be even. No such constraints exist if the boundaries are open.

If two spiral tips are connected by a wave front, the two spirals must rotate in opposite directions. Otherwise the wave front would have no distinct back and front side. Therefore, if the boundary condition is periodic, each clockwise spiral is connected to an anticlockwise spiral, so that all spirals form pairs. As time goes by, the specific spirals that pair in this way may change, however. Look, for example, at Fig. 13(b), and imagine that each of the end points of the wave fronts corresponds to a spiral tip. In the left panel, the upper left spiral tip is connected to the tip marked by a ring. In the right panel, when the two wave fronts have collided, the lower left tip is connected to the ring.

B. Wave front collision

In a frequency entrained state, two wave fronts that collide always annihilate. If they would pass through each other, the firing interval of an oscillator close to the collision point would be very small, as the forward and backward moving fronts sweep over the oscillator at a small time interval. The firing interval would then increase gradually as we move away from the collision point. In other words, the firing intervals would not all be the same, and there would be no frequency entrainment.

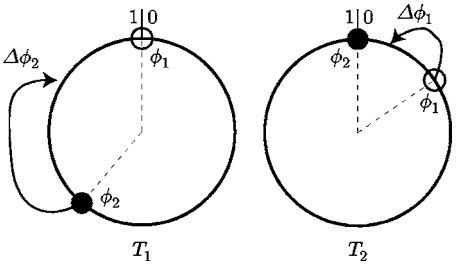

FIG. 20. Asymmetry of the interaction in model (1). The phase circle is shown at two consecutive times T_1 and T_2, and the phases ϕ_1 and ϕ_2 of two oscillators 1 and 2 are marked. We have $\Delta\phi_2 = gh[\phi_2(T_1)]$ and $\Delta\phi_1 = gh[\phi_1(T_2)]$. If we assume that the natural periods π_1 and π_2 are equal, the phases move around the circle with the same speed, and we get $\Delta\phi_1 = -(1-g)\Delta\phi_2$ from Fig. 1. A symmetric interaction would mean $\Delta\phi_1 = -\Delta\phi_2$.

There is nothing in model (1), however, that *a priori* prevents two wave fronts from passing each other or a wave front moving backward to be created in the wake of a forward moving wave front. In both cases, an oscillator a that fires at time T_a and triggers a neighbor b to fire at T_b, must in return be triggered by b to start a reverse wave. This can happen if the time difference $T_b - T_a$ is large enough so that ϕ_a has grown larger than ϕ_+ (Fig. 1) at time T_b. Naturally, this situation may occur if g is small (making $T_b - T_a$ large) and ϕ_+ is also small. It can be checked that a necessary condition is $\phi_+ \leqslant 1/[1 + \pi_{\min}\pi_{\max}^{-1}(1-g)^{-1}]$.

C. Entrained period and local coherence

We do not have a complete theory to explain the shape of the curves $\bar{p}(g)$ (Fig. 3) and $\bar{q}(g)$ (Fig. 7) in the concentric and spiral cases. However, we can account for some basic facts.

In the following, we assume that in any observed entrained state, oscillators receive pulses only when their phase belongs to one of the intervals $[0, \phi_-)$ and $(\phi_+, 1)$. Without rigorous proof, we claim that the state would otherwise be unstable [24]. We have $\phi' = \phi + gh(\phi)$, where ϕ and ϕ' are the phases of an oscillator just before and after it receives a pulse, respectively. A small phase perturbation $\delta\phi$ thus evolves according to $\delta\phi' = [1 + gh'(\phi)]\delta\phi$, and it will grow if $h'(\phi) > 0$. This is the case in the intermediate phase interval (ϕ_-, ϕ_+).

The entrained period $\bar{p}$ decreases when g increases. This is due to a basic asymmetry of the interaction in model (1). Namely, an oscillator 1 that fires before another oscillator 2 tends to advance the phase of 2 more than 2 retards the phase of 1 (Fig. 20). This asymmetry becomes more pronounced as g increases. The net acceleration of the lattice increases and $\bar{p}$ decreases. In the limit $g \to 1$, a firing oscillator triggers an immediate firing of all neighbors with phase $\phi \geqslant \phi_+$. The firing oscillator will not be retarded at all. Since this holds for all oscillators, we must have $\lim_{g\to 1} \bar{p} \leqslant \pi_{\min} = 1$. In a concentric landscape, there is a focus oscillator that may be retarded by its four neighbors, but is not accelerated by any neighbor. Thus $\lim_{g\to 1} \bar{p} \geqslant \pi_{\min}$, so that indeed $\lim_{g\to 1} \bar{p} = 1$. In a spiral landscape, the lower limit of $\bar{p}$ is set by the fact that the firing interval of an oscillator k cannot be less than $\phi_+\pi_k$. This value is taken if it is perturbed at $\phi_k = \phi_+$. Since all oscillators frequency entrain, we must have $\bar{p} \geqslant \phi_+\pi_{\max} = 3/4$.

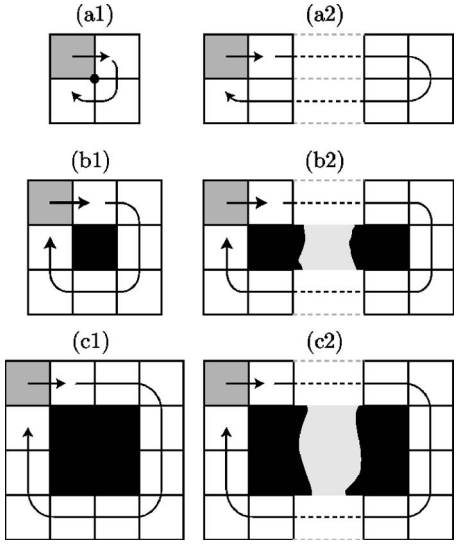

FIG. 21. The basic types of defects around which a spiral tip may rotate. Black cells correspond to quiescent oscillators. (a1) A point defect. (a2) A line defect. (b1) A quiescent oscillator, an oscillator defect. (b2) A row of quiescent oscillators, a row defect. (c1) A 2×2 block of quiescent oscillators. (c2) A $2\times n$ block of quiescent oscillators.

The local coherence measure $\bar{q}$ decreases toward zero as g increases, at least in the concentric case (Fig. 7). Basically, $\bar{q}$ is the mean time difference ΔT between firings of neighbor oscillators (i,j) and (k,l). Say that (i,j) fires before (k,l). The phase remaining after the advancing pulse from (i,j) before the firing state of (k,l) is reached is $1 - \phi'_{kl} = 1 - [\phi_{kl} + gh(\phi_{kl})] = (1-g)(1-\phi_{kl})$. We have $\Delta T \leqslant \pi_{\max}(1-\phi'_{kl})$, and thus $\bar{q}$ must decrease toward zero as $g \to 1$. This is true for spiral states also, provided they exist in this limit.

The entrained period $\bar{p}$ tends to be lower for spiral landscapes than for concentric landscapes, whereas $\bar{q}$ is higher. There is a simple reason for this relationship. To reduce the firing intervals more in spiral landscapes, the advancing pulses must be received at smaller phases, on the average, since the forward phase jumps $gh(\phi)$ then becomes larger. However, the remaining phase $1 - \phi'$ will then be larger, and therefore, ΔT and $\bar{q}$ will also be larger.

D. Spirals

In our terminology, a spiral tip always rotates around some kind of defect. Figure 21 shows the basic defect types. The type shown in row (c) has not been seen in the simulations, but cannot be ruled out. The thickness of a layer of quiescent oscillators can be two at the most, since all quiescent oscillators must abut an active oscillator in order to be kept quiescent. These structures should be seen as building blocks from which quite arbitrary defects can be constructed. First, line and row defects are most often curved. Second, we

have already mentioned that pieces of line and row defects are sometimes joined to form longer defects (Sec. III D). Third, we have also seen row defects that branch off. Fourth, it should be possible that defects form closed rings, although this has not been observed yet. It is noteworthy that a hypothetical ring of quiescent oscillators dynamically decouples the lattice into two independent parts—the interior and exterior of the ring.

Below, we try to account for the intervals of g in which different types of spirals appear. First, we give qualitative arguments, then we present some quantitative calculations.

The reason why spirals circling quiescent oscillators do not appear for low enough coupling strength g is that the quiescent oscillator must receive strong enough retarding pulses from its neighbors, so that its phase is kept below ϕ_- during one entrained period.

We see that spirals circling point defects disappear first as g increases (Fig. 14), then spirals circling an oscillator defect (Fig. 15) disappear. Then the oscillator row defect circled by the spiral apparently has to become longer and longer (Fig. 17) as g grows. The reason is the following: Consider the ring of oscillators that the spiral tip runs through in consecutive order. The time difference ΔT between the firings of neighbor oscillators on this ring has to decrease toward zero when g increases. The sum of all time differences should equal $\bar{p}$, but for high enough g this will no longer be possible. The longer the ring, the larger sum is possible. The spiral can survive at a larger g. In the case of a point defect, the ring of oscillators that the spiral tip runs through has length four; in the case of an oscillator defect, it has length eight; and if we are dealing with a row defect, the ring length increases from ten with the length of the row defect.

Let us make these arguments quantitative. First, we consider the lower bound for g in a row defect with M quiescent oscillators. Let δT_k be the largest time difference between successive pulses received by a quiescent oscillator k, and let m_k be the number of pulses received by k during the entrained period $\bar{p}$. We have

$$\delta T_k \geqslant \bar{p}/m_k, \quad \forall\, k. \tag{9}$$

To keep k in the phase interval $(0,\phi_-)$, it is most favorable to perturb it at phase $\phi_k=\phi_-$, since then the backward phase jump $gh(\phi_k)=-g\phi_k$ is the largest. Then, we must perturb it again within a time $\pi_k g\phi_-$, otherwise ϕ_k escapes the interval $(0,\phi_-)$. Thus, we must have

$$\delta T_k \leqslant \pi_k g\phi_-, \quad \forall\, k, \tag{10}$$

or $g \geqslant \bar{p}/(m_k\pi_k\phi_-)$ from Eq. (9). Let m be the minimum m_k in the row. Then, we have to require $g \geqslant \bar{p}/(m\pi_k\phi_-)$. Since $\bar{p} \geqslant \pi_{\max}\phi_+$, we get the lower bound

$$g \geqslant \frac{\phi_+}{m\phi_-}. \tag{11}$$

For an oscillator defect, we have $m=4$; for a straight row defect of length $M=2$, we have $m=3$; and for a longer straight row defect, we have $m=2$.

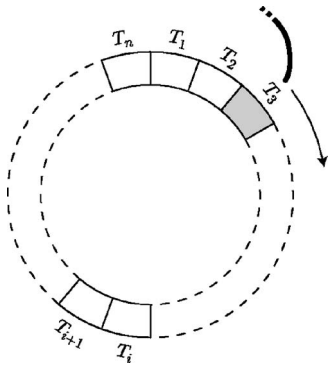

FIG. 22. The oscillator ring that the spiral tip runs through. The interior may contain a point defect, an oscillator defect, a row defect, or possibly a line defect.

Consider now the upper bound for different spiral types. Label the oscillators in the ring $1,2,\ldots,n$ and let them fire at times $T_1 \leqslant T_2 \leqslant \cdots \leqslant T_n \leqslant T_1+\bar{p}$ (Fig. 22). Then define $\Delta T_k = T_{k+1}-T_k$, with $\Delta T_n = T_1+\bar{p}-T_n$. Let ϕ_k^b be the phase of oscillator k just before $k-1$ fires. We have

$$\Delta T_{k-1} \leqslant \pi_k\{1-[\phi_k^b + gh(\phi_k^b)]\} = \pi_k(1-g)(1-\phi_k^b). \tag{12}$$

The inequality should be an equality if no neighbor to k outside the ring fires between $k-1$ and k, and a strict inequality if some neighbor does fire. Since we must have $\phi_k^b > \phi_+$, it follows that

$$\Delta T_{k-1} \leqslant \pi_{\max}(1-g)(1-\phi_+), \quad \forall\ k. \tag{13}$$

For some j, we must have $\Delta T_j \geqslant \bar{p}/n$, and since $\bar{p} \geqslant \pi_{\max}\phi_+$, we may write

$$\exists\ j, \quad \Delta T_j \geqslant \pi_{\max}\phi_+/n. \tag{14}$$

Taken together, Eqs. (13) and (14) imply

$$g \leqslant 1-\frac{\phi_+}{n(1-\phi_+)}. \tag{15}$$

Equations (11) and (15) express upper and lower bounds for the g intervals in which different types of spirals occur. The actual intervals are more narrow. More accurate upper limits of g can be estimated by ignoring the rest of the lattice, treating the ring in Fig. 22 as a one-dimensional lattice with periodic boundary condition. For each k, we have

$$\pi_k = \bar{p} + g(1-g)^{-1}\Delta T_{k-1} - g\Delta T_k \tag{16}$$

(with $\Delta T_0 \equiv \Delta T_n$). Summing all n equations and using

$$\bar{p} = \sum_k \Delta T_k, \tag{17}$$

we get

$$\sum_{k=1}^{n} \pi_k = [n + g^2(1-g)^{-1}]\bar{p}. \tag{18}$$

We see that this equation only has allowed solutions for small enough g, otherwise $\bar{p}$ becomes smaller than the mini-

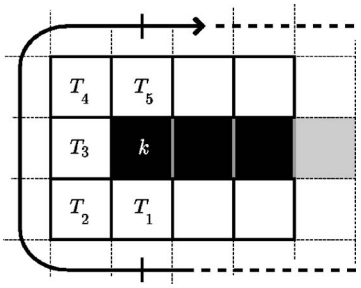

FIG. 23. Illustration that helps understand the argument why row defects are forbidden for high enough g. $\Delta T_j = T_{j+1} - T_j$, where T_j is the firing time for oscillator j and $j = 1,2,3,4,5$.

mum allowed value $[1-g(1-\phi_+)]\max\{\pi_k\}$. To maintain $\bar{p}$ large as g increases, all ΔT_k should be maintained large, according to Eq. (17). To do this, ϕ_k^b has to decrease, according to Eq. (12). The maximum allowed g is thus the one for which $\Delta T_k = \pi_k(1-g)(1-\phi_+)$ for each k. Inserting this expression in Eq. (18), again using Eq. (17), we get

$$g \leqslant n/2 \pm \sqrt{n^2/4 - n + (1-\phi_+)^{-1}}. \tag{19}$$

In this way, we obtain $g \leqslant 2-\sqrt{2} \approx 0.59$ for spirals circling a point defect ($n=4$), and $g \leqslant 4-\sqrt{10} \approx 0.84$ for spirals circling an oscillator defect ($n=8$). These values are in good agreement with the numerical data (Figs. 14 and 15).

In Eq. (15), we see that the length n of the ring that the spiral tip runs through (Fig. 22) has to increase as g grows toward 1. An interesting question is whether spiral landscapes are possible in the limit $g \to 1$. Then the length of the line or row defects must diverge. We see no reason why this is cannot happen for line defects, but below we show that spirals circling row defects are impossible above a certain value of g.

Consider a quiescent oscillator k at one end of the row defect (Fig. 23). It gets three retarding pulses as the wave front passes. Then it has to wait until the front returns before it gets another retarding pulse. The critical condition is that this time interval I has to be small enough so that ϕ_k does not grow larger than ϕ_- in the meantime. We have to require $I \leqslant \phi_- \pi_k \leqslant \phi_- \pi_{\max}$. We have $I = \bar{p} - (\Delta T_1 + \Delta T_2 + \Delta T_3 + \Delta T_4)$. From Eq. (12), we have $\Delta T_j \leqslant \pi_{\max}(1-g)(1-\phi_+)$. Since $\bar{p} \geqslant \phi_+ \pi_{\max}$, we may write $I \leqslant \phi_+ \pi_{\max} - 4\pi_{\max}(1-g)(1-\phi_+)$. Using $I \leqslant \phi_- \pi_{\max}$, we get $g \leqslant 1 - (1/4)(\phi_+ - \phi_-)(1-\phi_-)^{-1}$. For our parameter values, we get $g \leqslant 0.95$.

E. Other models

In the case of identical oscillators, $\pi_{ij} = 1$, $\forall\, ij$, the spiral landscapes acquire the minimum possible period $\bar{p} = \phi_+ \pi_{\max} = 0.5$ in the limit $g \to 1$, just as in the case of diverse oscillators (cf. Sec. IV C). It is easy to see that there is always a coherent state with $\bar{p} = \pi_{ij} = 1$. However, one may ask if there are concentric landscapes with foci. This can be excluded by the following argument. If there is a focus, then there is an oscillator that is retarded by some neighbors and not accelerated by any. Thus, $\bar{p} > 1$. But if there is a focus, for topological reasons there must also be an "antifocus," an oscillator that is accelerated by some neighbors, but not retarded by any. Therefore, $\bar{p} < 1$, and we have a contradiction. The absence of concentric landscapes with foci explains the absence of spiral landscapes correlated to such landscapes. For periodic boundary conditions it is strictly true that there cannot be any correlations, since then all oscillator sites are equivalent, and no preferred spiral position can exist.

Let us explain some of the differences between models (1) and (7) (Fig. 19). For the latter model, there is no tendency that $\bar{p}$ in concentric landscapes approaches $\pi_{\min} = 1$ as K increases, whereas this is bound to happen in model (1) (Sec. IV C). For any given K, we can adjust the phase differences $\phi_{kl} - \phi_{ij}$ between neighbor oscillators so that $\dot{\phi}_{ij}$ takes any desired value in the range $[\pi_{ij}^{-1} + K\Sigma \min\{\Gamma(x)\}, \pi_{ij}^{-1} + K\Sigma \max\{\Gamma(x)\}]$. The width of this interval clearly grows without bound as K increases. For concentric landscapes, however, we must have $\pi_{\min} < \bar{p} < \pi_{\max}$. For our choice of $\Gamma(x)$, there will be a focus oscillator that is always retarded, so that $\bar{p} > \pi_{\min}$, and an antifocus oscillator that is always accelerated, so that $\bar{p} < \pi_{\max}$. In a similar way, the phase differences do not have to decrease as K grows, in contrast to model (1), where we approach the coherent state as $g \to 1$ (Fig. 20). Consequently, we see that the local coherence measure $\bar{q}'$ does not decrease for spiral landscapes as K increases.

The fact that the phase differences do not have to decrease means that there is no value of K above which spirals circling point defects are impossible. In contrast, oscillator defects are absent altogether. The concept of a "quiescent oscillator" is meaningless, since there is nothing special with $\phi_{ij} = 0$ in model (7). Equation (7) is left invariant if we shift the frequency zero by an arbitrary amount α, i.e., if we make a change of variables $\phi'_{ij} = \phi_{ij} + \alpha t$ and $\omega'_{ij} = \omega_{ij} + \alpha$ for all (i,j).

V. DISCUSSION

Maybe the most fundamental question raised in this study is whether a partly coherent phase exists in the thermodynamic limit $N \to \infty$. Our results indicate that this is not the case in our model. This conclusion is based on two findings. The first is that the wavelength is independent of lattice size (Fig. 8). The second is that the focus density in concentric landscapes drops when the lattice size increases (Fig. 10). Let us discuss why these properties make a coherent phase less probable. Figure 24 shows associated firing times T in a medium with a continuous space variable x. The local minima correspond to foci. The gradient $|dT/dx|$ corresponds to $\bar{q}$. If the curve is contained in an interval DT that is smaller than $\bar{p}$, then partial coherence is expected. If the focus density is independent of lattice size, then DT and the degree of coherence may also be independent of lattice size, and a partly coherent phase is possible. Then we can choose a large enough $g < 1$, so that $\bar{q}$ becomes small enough and $DT \ll \bar{p}$. If we then let $N \to \infty$, we will have a partly coherent state. In contrast, if the density decreases (lower curve), then DT will increase with N for a given g and $\bar{q}$. The degree of coherence decreases. If the focus density $\rho \to 0$ as $N \to \infty$, then we can rule out a partly coherent phase. However, if it

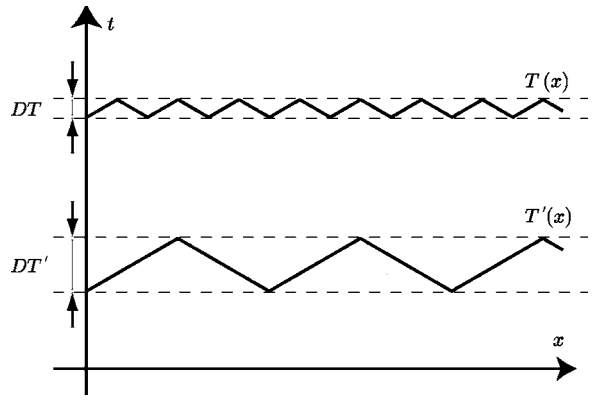

FIG. 24. Illustration of the coherence discussion. We can associate two firing events, at times T_a and T_b, of neighbor oscillators a and b, if one event triggers the other. In the one-dimensional case, we can form a chain of associated firing times T. In a continuous version of the medium, this chain forms a curve $T(x)$. See text for further explanation.

stabilizes at a small nonzero value, we cannot be certain. But this does not guarantee the existence of a coherent phase. Figure 24 shows an idealized situation where dT/dx is constant and the foci are evenly spaced. If this is not the case, it is probable that $T(x)$ will show diffusion-like properties and will not be bounded as $x \to \infty$.

Another significant finding, in our view, is the way the probability to get concentric and spiral landscapes depends on lattice size N and coupling strength g (Fig. 4). In Sec. III E, we discuss how this leads to hysteresis effects. This behavior may be of importance in relation to sinus node reentry (Sec. I). The sudden frequency increase and the circular excitation waves seen in this syndrome suggests that it corresponds to the appearance of a spiral landscape within the sinus node. It may then be possible to return to a healthy concentric landscape by making use of the hysteresis. Namely, we may gradually increase intercellular coupling to the point where the system spontaneously jumps to a concentric state, and then gradually reduce coupling back to normal values, staying on the concentric arm (Fig. 3). (Methods to alter coupling are discussed, e.g., in Ref. [25].)

There is, however, a potential hazard with this scheme. If we are unable to raise coupling high enough, we may become stuck in the apparently nonfrequency entrained spiral landscapes appearing for very high g, described in Sec. III E. Why do these landscapes appear? Since row defects are much more common than line defects, the system typically displays stable row defects before entering the very high coupling regime. Now, in Sec. IV D, we show that row defects are forbidden in frequency entrained states for $g > 0.95$. Since the system has a memory of row defects, for higher g the system might, therefore, approach a nonfrequency entrained state containing nonstationary row defects. We cannot rule out that these states correspond to very long chaotic transients.

Let us briefly discuss why the sinus node may end up in a spiral landscape in the first place. The autonomous nervous system innervates the sinus node and controls heart rate through release of acetylcholine and norepinephrine at the nerve endings. Sudden changes in the concentration of these neurotransmitters ought to "shake" the system, leaving it far from a stable frequency entrained state. It may then be attracted to a new stable state, possibly a spiral landscape. Abnormally weak intercellular coupling within the node may, therefore, facilitate the appearance of sinus node reentry, since spiral states then become more probable (Fig. 4).

Although we are not aware of any other systematic study of waves in discrete oscillatory media, there has been a lot of effort to understand spiral waves in discrete *excitable* media. In particular, the phenomenon of *spiral wave breakup* has been studied in detail, since it is a possible cause of fatal cardiac arrhythmia [26,27]. The resulting wave patterns are typically disordered and aperiodic in both space and time. In contrast, we typically see wave patterns that are spatially disordered [Fig. 2(c)], but perfectly periodic in time. Of course, in the nonfrequency entrained regime, we see solutions that are temporally aperiodic as well. Then, spiral tips are often stationary for a long time and then suddenly move. In an excitable medium, there can be no asymptotic solution containing concentric waves (unless external pacing is introduced). On the other hand, the static solution where the medium is at rest does not exist in our system. An oscillator can only be kept quiescent by a nearby, active oscillator. This fact makes extended inactive spiral cores impossible (Fig. 21), even if they are often seen in excitable media [28].

One may ask which of the observed properties are due to the fact that the oscillators have heterogeneous natural periods. First, as noted in Sec. III F, if the oscillators are identical, *all* observed states are frequency entrained, regardless the coupling strength g. Second, there appear *no* concentric landscapes (Sec. IV E). Their role is played by coherent landscapes (with $\bar{q}=0$). The question whether partial coherence is possible for finite $g<1$ in the thermodynamic limit $N \to \infty$ becomes superfluous, since coherent landscapes exist for any N. However, it seems that the *probability* to get a coherent landscape for random initial condition is nevertheless zero in the limit $N \to \infty$ (cf. Fig. 4). A third difference is that there are no correlations between phase landscapes obtained for different g or different random initial conditions. This is because there are no variations in a fixed natural period landscape to which the phase landscape can correlate. An important *similarity* between heterogeneous and homogeneous lattices is that the probability to get spiral or nonspiral landscapes seems to depend in the same way on g and N. Also, the possible spiral types are the same.

Our findings are of interest mainly if they are fairly model independent. The Kuramoto-like model (7) that we simulated for comparison showed some similarities and some differences. However, we may argue that our model, with a diffusive, pulse-like interaction that tends to decrease phase and frequency differences, is more similar to real oscillator networks, at least to those in the biological applications. Further, model (7) is the universal form of an oscillator network in the *low coupling* limit, whereas this study deals with the *high coupling* regime. A good test to determine the generality of the results could be to study the Winfree model in the form used by Ariaratnam and Strogatz [3], where our PRC (Fig. 1) is replaced by $-\sin(2\pi\phi)$ and the delta spike interaction $\delta(\phi)$ is replaced by the smooth function $1+\cos(2\pi\phi)$.

[1] A. T. Winfree, *The Geometry of Biological Time* (Springer, New York, 1980); A. Pikovsky, M. Rosenblum, and J. Kurths, *Synchronization: A Universal Concept in Nonlinear Science* (Cambridge University Press, Cambridge, 2001); S. Strogatz, *Sync: The Emerging Science of Spontaneous Order* (Hyperion, New York, 2003).
[2] Y. Kuramoto, *Chemical Oscillations, Waves and Turbulence* (Springer, Berlin, 1984).
[3] A. T. Winfree, J. Theor. Biol. **16**, 15 (1967); P. C. Matthews, R. E. Mirollo, and S. H. Strogatz, Physica D **52**, 293 (1991); W. Senn and R. Urbanczik, SIAM J. Appl. Math. **61**, 1143 (2000); J. T. Ariaratnam and S. H. Strogatz, Phys. Rev. Lett. **86**, 4278 (2001); S. De Monte, F. d'Ovidio, and E. Mosekilde, Phys. Rev. Lett. **90**, 054102 (2003).
[4] S. H. Strogatz and R. E. Mirollo, Physica D **31**, 143 (1988); H. Daido, Phys. Rev. Lett. **61**, 231 (1988); N. Kopell and G. B. Ermentrout, SIAM J. Appl. Math. **50**, 1014 (1990).
[5] P. Östborn, Phys. Rev. E **66**, 016105 (2002).
[6] P. Östborn, Phys. Rev. E **70**, 016120 (2004).
[7] P. Östborn, S. Åberg, and G. Ohlén, Phys. Rev. E **68**, 015104(R) (2003).
[8] W. K. Bleeker *et al.*, Circ. Res. **46**, 11 (1980).
[9] P. L. Carlen *et al.*, Brain Res. Rev. **32**, 235 (2000).
[10] C. S. Colwell, J. Neurobiol. **43**, 379 (2000).
[11] O. Kiehn *et al.*, Brain Res. Bull. **53**, 649 (2001).
[12] K. T. Moortgat, T. H. Bullock, and T. J. Sejnowski, J. Neurophysiol. **83**, 971 (2000); **83**, 984 (2000).
[13] J. Buck, Q. Rev. Biol. **63**, 265 (1988).
[14] M. C. Cross and P. C. Hohenberg, Rev. Mod. Phys. **65**, 851 (1993).
[15] A. F. Taylor, Prog. React. Kinet. **27**, 247 (2002).
[16] I. S. Aranson and L. Kramer, Rev. Mod. Phys. **74**, 99 (2002).
[17] H. Guo, L. Li, H. Wang, and Q. Ouyang, Phys. Rev. E **69**, 056203 (2004).
[18] H. Sakaguchi, S. Shinomoto, and Y. Kuramoto, Prog. Theor. Phys. **79**, 1069 (1988).
[19] T. Aoyagi and Y. Kuramoto, Phys. Lett. A **155**, 410 (1991).
[20] J. A. Gomes, D. Mehta, and M. N. Langan, PACE **18**, 1045 (1995).
[21] T. Sano, T. Sawanobori, and H. Adaniya, Am. J. Physiol. **235**, H379 (1978); J. Jalife *et al.*, *ibid.* **238**, H307 (1980); J. M. B. Anumonwo *et al.*, Circ. Res. **68**, 1138 (1991).
[22] B. I. Shraiman, Phys. Rev. Lett. **57**, 325 (1986).
[23] If the chain has periodic boundary conditions, we may have $\oint_c \nabla \phi \cdot dl = m > 0$, where c is the closed chain itself [cf. Eq. (2)]. This might be interpreted as a spiral, in particular if there are no foci present.
[24] In the one-dimensional case, it is proved in Ref. [5] that an entrained state fulfilling the assumption is indeed stable.
[25] S. A. Jones, M. K. Lancaster, and M. R. Boyett, J. Physiol. (London) **560**, 429 (2004).
[26] H. Ito and L. Glass, Phys. Rev. Lett. **66**, 671 (1991).
[27] G. Bub, A. Shrier, and L. Glass, Phys. Rev. Lett. **88**, 058101 (2002).
[28] *Computational Biology of the Heart*, edited by A. V. Panfilov and A. V. Holden (John Wiley & Sons, New York, 1997).